



HAL
open science

Basin-scale biogeochemical and ecological impacts of islands in the tropical Pacific Ocean

Monique Messié, Anne Petrenko, Andrea M. Doglioli, Elodie Martinez, Séverine
Alvain

► **To cite this version:**

Monique Messié, Anne Petrenko, Andrea M. Doglioli, Elodie Martinez, Séverine Alvain. Basin-scale biogeochemical and ecological impacts of islands in the tropical Pacific Ocean. *Nature Geoscience*, 2022, 15, pp.469-474. <10.1038/s41561-022-00957-8>. <insu-03779397>

HAL Id: insu-03779397

<https://insu.hal.science/insu-03779397v1>

Submitted on 22 Dec 2022

HAL is a multi-disciplinary open access archive for the deposit and dissemination of scientific research documents, whether they are published or not. The documents may come from teaching and research institutions in France or abroad, or from public or private research centers.

L'archive ouverte pluridisciplinaire **HAL**, est destinée au dépôt et à la diffusion de documents scientifiques de niveau recherche, publiés ou non, émanant des établissements d'enseignement et de recherche français ou étrangers, des laboratoires publics ou privés.



HAL Authorization

1 *This version of the article has been accepted for publication, after peer review and is subject to*
2 *Springer Nature's AM terms of use, but is not the Version of Record and does not reflect post-*
3 *acceptance improvements, or any corrections. The Version of Record is available online at:*
4 <https://doi.org/10.1038/s41561-022-00957-8> (full text: <https://rdcu.be/cO4qr>)

5 Citation: Messié, M., Petrenko, A., Doglioli, A.M., Martinez, E., and Alvain, S. Basin-scale
6 biogeochemical and ecological impacts of islands in the tropical Pacific Ocean. Nat. Geosci. 15,
7 469–474 (2022). <https://doi.org/10.1038/s41561-022-00957-8>

8

9

10 Basin-scale biogeochemical and ecological impacts of islands in the
11 tropical Pacific Ocean

12

13 M. Messié^{1,2,*}, A. Petrenko², A. Doglioli², E. Martinez³, and S. Alvain⁴

14

15 ¹Monterey Bay Aquarium Research Institute, Moss Landing, CA 95039, USA

16 ²Aix Marseille Univ, Université de Toulon, CNRS, IRD, MIO, Marseille, France

17 ³University of Brest, Ifremer, CNRS, IRD, Laboratoire d'Océanographie Physique et Spatiale
18 (LOPS), IUEM, 29200 Brest, France

19 ⁴Laboratoire d'Océanologie et de Géosciences, UMR 8187 – LOG, CNRS, Université de Lille,
20 Université du Littoral Côte d'Opale, Wimereux, France

21 *corresponding author, monique@mbari.org

22

23 **In the relatively unproductive waters of the tropical ocean, islands can enhance**
24 **phytoplankton biomass and create hotspots of productivity and biodiversity that sustain**
25 **upper trophic levels, including fish that are crucial to the survival of islands' inhabitants.**
26 **This phenomenon, coined the "island mass effect" sixty-five years ago, has been widely**
27 **described. However, most studies focused on individual islands, and very few documented**
28 **phytoplankton community composition. Consequently, basin-scale impacts on**
29 **phytoplankton biomass, primary production, and biodiversity remain largely unknown.**
30 **Here we systematically identify enriched waters near islands from satellite chlorophyll**
31 **concentration (a proxy for phytoplankton biomass) to analyze the island mass effect for all**
32 **tropical Pacific islands on a climatological basis. We find enrichments near 99% of islands,**
33 **impacting 3% of the tropical Pacific Ocean. We quantify local and basin-scale increases in**
34 **chlorophyll and primary production by contrasting island-enriched waters with nearby**
35 **waters. We also unveil, for the first time, a significant impact on phytoplankton community**
36 **structure and biodiversity visible in anomalies in the ocean color signal. Our results suggest**
37 **that, in addition to strong local biogeochemical impacts, islands may have even stronger**
38 **and further reaching ecological impacts.**

39 Phytoplankton, the tiny drifting algae that fix carbon dioxide via photosynthesis, are responsible
40 for about half of the world's primary production¹ and support essentially all life in the open
41 ocean. Their community composition and biodiversity have been tied to vertical carbon export,
42 resource use efficiency, and ecological stability^{2,3,4}. As such, phytoplankton biomass, production,
43 and biodiversity have far-reaching impacts on marine ecosystems and the global carbon cycle. It
44 is thus paramount to understand their environmental drivers so as to predict, and potentially
45 mitigate, how they may change in the future. In most of the tropical ocean, nutrient supply is the

46 primary factor limiting phytoplankton growth⁵. Far from continents, nutrients are brought to the
47 sunlit surface layer primarily by vertical mixing⁶, wind- and eddy-driven upwelling⁷, atmospheric
48 deposition⁸, nitrogen fixation⁹, and horizontal advection¹⁰. Phytoplankton biodiversity is difficult
49 to monitor; its patterns and drivers remain largely unknown even when focusing on the simplest
50 of biodiversity metrics, richness (number of coexisting species). Several studies found high
51 richness in warm, stable tropical regions and identified temperature as the primary phytoplankton
52 richness driver^{11,12}. Others described increased richness in dynamic regions¹³, highlighting
53 drivers such as nutrient supply rate and composition, advection, and top-down control¹⁴.

54 Here, we focus on a phenomenon that has paradoxically received little attention at the basin
55 scale, despite its prevalence and strong local impacts: island-driven increases in phytoplankton
56 production, resulting in nearly ubiquitous chlorophyll enrichments near tropical Pacific islands
57 and atolls¹⁵. This “island mass effect” (IME)¹⁶ can result from various processes such as
58 upwelling and mixing in lee eddies, island runoff, submarine groundwater discharge, and others
59 (reviewed by Gove et al.¹⁵). These processes supply additional nutrients relative to surrounding
60 waters, supporting enhanced phytoplankton growth and dramatically increasing local
61 productivity. The resulting increased fish production is crucial to Pacific island societies that rely
62 on fishing for food security and protein intake¹⁷. By increasing primary production, islands can
63 also locally create an important oceanic sink for atmospheric CO₂ (as observed in the Southern
64 Ocean¹⁸) and have been hypothesized to significantly contribute to the global carbon budget¹⁹.

65 IMEs have been described for a few of the thousands of tropical Pacific islands, notably the
66 Galapagos²⁰, Hawaii²¹, the Marquesas²², Kiribati²³, Solomon²⁴, New Caledonia²⁵, Tonga²⁶,
67 Vanuatu, and Fiji²⁷. There are also some rare reports of island impacts on phytoplankton
68 community composition^{28,29,30}. Only two studies systematically investigated the IME for several

69 islands at once: a compilation of *in situ* chlorophyll concentration in the south tropical Pacific²⁷,
70 and an analysis of satellite chlorophyll increase near 35 coral reef islands and atolls¹⁵. Neither
71 study considered phytoplankton community composition. A systematic study of the IME for all
72 islands in the tropical Pacific, particularly addressing impacts on phytoplankton biodiversity, is
73 unprecedented.

74 **Characterizing island mass effects in the tropical Pacific**

75 We investigated the IME for all tropical Pacific islands and shallow reefs using satellite surface
76 chlorophyll concentrations (hereafter Chl). A total of 11,449 islands and 4,602 shallow reefs
77 were identified from high-resolution coastline and bathymetry. Islands and reefs were combined
78 within land pixels of the 4 km resolution Chl grid (pixels shallower than 30 m were treated as
79 land, see Methods), resulting in a database of 437 islands and 227 shallow reefs (hereafter
80 “islands”). An algorithm automatically detecting IMEs from Chl maps was developed and
81 applied both to the time-averaged Chl and to a monthly climatology. For each island, the
82 algorithm identified the IME as a Chl contour enclosing the island and surrounding high-Chl
83 waters, termed IME region. A reference (REF) region of the same size was detected alongside
84 each IME region, enclosing nearby non-IME waters (Extended Fig. 1). The REF region
85 represents conditions that would exist if no IME was present. Increases in Chl nearby islands and
86 within the IME regions were defined relative to REF.

87 The algorithm detected IMEs for most islands, whether in oligotrophic gyres or in more
88 productive equatorial regions. Islands with the strongest, most far-reaching impacts on average
89 Chl include the Marquesas, Fiji/Tonga, Solomon, Kiribati, and the Galapagos (Fig. 1). Most
90 IMEs are strongly seasonal, such that an average map does not adequately render the IME

91 prevalence or strength. When applied to climatological maps (Fig. 1 inserts), the method detected
92 an IME near 99% of islands (Table 1). Some of these IMEs only represent weak Chl increases
93 because climatological averages smooth the IME signal, but their presence indicates that an IME
94 likely occurred during the satellite time period. A more conservative approach still identified
95 IMEs near 90% of islands (right column). If anything, the IME prevalence may be
96 underestimated as small IMEs may not be detected using a 4-km resolution product (see Table
97 S1). This confirms that the IME is nearly ubiquitous in the tropical Pacific¹⁵. Overall, our results
98 indicate that the IME impacts 3% of the tropical Pacific area although islands and reefs together
99 only represent 0.4%.

100 **Island impacts on phytoplankton biomass and production**

101 Local IME impacts were assessed by comparing the paired IME and REF regions, and total
102 impacts calculated by summing the results over the entire tropical Pacific for each climatological
103 month and averaging over time. The results reveal a strong impact of islands on surface
104 phytoplankton biomass (using Chl as a proxy) and on satellite-derived primary production³¹
105 (Table 1). Chl increases by 9% and primary production by 3% on average within IME regions.
106 Next to the islands, impacts are even more dramatic with a Chl increase of 26% on average. The
107 apparent higher impact on Chl than primary production is partially due to the lower spatial
108 resolution of the primary production product (9 km vs 4 km for Chl), combined with the fact that
109 pixels closest to islands, where impacts are greatest, must be removed (see Methods).

110 While local impacts are very high, islands seem to increase Chl and primary production by less
111 than 1% over the tropical Pacific (Table 1). These numbers may be underestimated because of
112 removing shallow pixels near islands where impacts are greatest, and because our algorithm

113 misses delayed IMEs occurring offshore²⁶ by assuming that the IME region is connected to the
114 island. Although Chl measured by satellites is only representative of approximately a fifth of the
115 euphotic zone, the relative impact on total vertically integrated phytoplankton biomass may be
116 expected to be of the same order of magnitude as the impact on Chl since IME enrichments
117 typically occur over the full euphotic zone¹⁵.

118 The overall primary production increase around 0.05 PgC/yr (Table 1) can be compared to other
119 processes, for which regional estimates of the nitrate supply carbon-equivalent (potential new
120 production) are available. Potential new production represents an upper bound for new
121 production, itself representing less than half of primary production in the region³², which
122 provides a basis for rough comparisons with the IME even though island-induced nutrient supply
123 is unknown. These other processes include wind-driven upwelling (1.8 to 3.9 PgC/yr including
124 equatorial upwelling when adapting past results to the region³³), turbulent vertical mixing at the
125 nitracline (0.4 PgC/yr for the region⁶), nitrogen fixation (around 0.2 PgC/yr for the Pacific³⁴,
126 noting that nitrogen fixation may be partly supported by IMEs^{28,26}), and the Peru upwelling
127 system (0.1 PgC/yr³⁵). Consequently, despite strong local impacts, islands are unlikely to
128 represent a major source of nutrients for phytoplankton in the tropical Pacific and to play an
129 important role in the global carbon budget.

130 **Island impacts on phytoplankton taxonomy**

131 Assessing island impacts on phytoplankton species composition is a challenging proposition.
132 There is at present no *in situ* dataset with the taxonomic and spatiotemporal coverage needed to
133 describe phytoplankton community structure and biodiversity throughout the tropical Pacific.
134 Significant progress has been made towards identifying phytoplankton taxonomy from space³⁶,

135 but published methods only identify a small number of broad taxonomic groups or size classes.
136 To circumvent the lack of taxonomic resolution in satellite products, we used PHYSAT³⁷, a
137 method clustering anomalies in the ocean color signal into 61 phenological bio-optical classes³⁸
138 (hereafter phenoclasses, see Methods). Because phytoplankton characteristics such as cell size,
139 composition, intracellular structure, cell arrangement, and absorption impact the ocean color
140 signal, phenoclasses are representative of various phytoplankton communities³⁹. We applied
141 classical ecological metrics to phenoclasses, capturing changes in phenoclass composition and
142 diversity between IME and REF regions. These ecological metrics describe island-driven
143 changes in phenoclasses, themselves revealing changes in phytoplankton taxonomy.

144 Island impacts on phytoplankton community composition were studied using the Bray-Curtis
145 dissimilarity index applied to phenoclasses (Fig. 2a). High phenoclass dissimilarity was
146 identified between IME and REF regions for most islands, particularly at low latitudes,
147 suggesting a strong island impact on phytoplankton community composition. These differences
148 are considerably higher than between random sets of pixels encompassing the IME and REF
149 regions (Fig. 3a left), confirming that they are significant and not due to random spatial
150 heterogeneity in PHYSAT phenoclasses. We looked more closely at the most common
151 phenoclasses found in the tropical Pacific. These are part of “labeled” phenoclasses that were
152 matched to dominant broad taxonomic groups thanks to coincident in situ data. The
153 corresponding phytoplankton groups are mostly *Prochlorococcus*, followed by nanoplankton and
154 *Synechococcus*, consistent with known phytoplankton composition in the region⁴⁰.

155 *Prochlorococcus*-labeled phenoclasses significantly decreased in proportion within the IME
156 region relative to REF, while *Synechococcus*- and nanoplankton-labeled phenoclasses both

157 increased, albeit non-significantly for nanoplankton (Fig. 3a right). This is coherent with reports
158 of *Synechococcus* and nanoplankton outcompeting *Prochlorococcus* at higher nutrient levels^{41,42}.

159 Island impacts on phytoplankton biodiversity were investigated using several dimensions of
160 phenoclass diversity: richness (number of distinct phenoclasses), evenness (phenoclass
161 proportion homogeneity), and the Shannon index, a widely used biodiversity metric that accounts
162 for both richness and evenness (Table 1). On average, phenoclass richness strongly increases
163 near islands, more than Chl and primary production. The island-driven phenoclass richness
164 increase is spatially variable (Fig. 2b), highest poleward of 10° latitude in both hemispheres.

165 There is no impact on evenness, and a smaller impact on Shannon diversity. Part of the richness
166 increase simply arises because, by definition, Chl is higher in IME than REF regions (Fig. 3b,
167 left). Indeed, phenoclass richness is strongly correlated with Chl ($r = 0.72$ across REF regions,
168 Extended Fig. 3), consistent with *in situ* phytoplankton richness patterns in low productivity
169 waters⁴³. However, the island-driven increase in phenoclass richness is only weakly correlated to
170 the Chl increase ($r = 0.22$), suggesting that this Chl signal only explains part of the phenoclass
171 richness increase. We randomly selected two thirds of the IME and REF regions with similar Chl
172 characteristics, effectively removing the Chl signal (Extended Fig. 4). A total of 1,000 random
173 permutations were selected, and 33% of permutations still displayed significantly higher
174 phenoclass richness within the IME subset (Fig. 3b, right). Taken together, these results suggest
175 that the observed island-driven increase in phenoclass richness is not only linked to increased
176 Chl, but also partly due to some island-specific phenomenon. We hypothesize that some islands
177 release nutrients with ratios different from the ones of ambient waters, depending on soil
178 composition and human activities, which could favor different species and increase
179 phytoplankton richness¹⁴. By contrast, weaker taxonomic impacts would be expected near

180 seamounts⁴⁴, because seamount-driven enrichments result from upwelling and mixing⁴⁵ of water
181 masses close to Redfield ratios.

182 Our satellite-based findings provide compelling evidence for a strong IME impact on
183 phytoplankton community composition and biodiversity. While PHYSAT is only a proxy for
184 phytoplankton taxonomy, our results match previous reports from the Marquesas islands,
185 including a shift from *Prochlorococcus* to *Synechococcus* and an increase in phytoplankton
186 biodiversity leeward of the islands^{29,30}. This island-driven increase in phytoplankton biodiversity
187 may be a crucial piece contributing to islands being biodiversity hotspots in the world oceans⁴⁶.
188 Island effects could also contribute to the observed latitudinal maximum phytoplankton richness
189 in the tropics^{11,12}, since islands can export biodiversity to surrounding waters⁴⁶. Observations of
190 phytoplankton taxonomy around other islands are needed to confirm PHYSAT-inferred island
191 impacts on phytoplankton community composition and biodiversity.

192 Regardless of impacts on phytoplankton taxonomy, local impacts on biomass and productivity
193 are so high that regions enriched by IMEs represent oases in an otherwise largely unproductive
194 environment (Fig. 1). There is strong evidence that they attract fish and marine predators^{47,48}, and
195 represent important stopovers along marine migration corridors⁴⁹. While fishery data would be
196 biased for islands (due to confounding effects of higher fish biomass and proximity), a recent
197 study of seamounts found a more than doubled fish catch at seamounts with Chl enhancements
198 relative to seamounts without⁴⁵. Some islands such as Hawaii and the Galapagos also represent
199 key conservation sites deemed irreplaceable because of the presence of endemic marine
200 species⁵⁰. This suggests that islands have profound ecological consequences both at the local and
201 basin scale, even though large-scale impacts on primary production appear to be small.

202

203 **Acknowledgements**

204 M.M. was funded by the European Union’s Horizon 2020 research and innovation programme
205 under the Marie Skłodowska-Curie grant agreement SAPPHIRE No. 746530, and by the David
206 and Lucile Packard Foundation. The project leading to this publication has received funding from
207 European FEDER Fund under project 1166-39417 (M.M., A.P., A.D.). We thank Anne-Hélène
208 Rêve-Lamarche and David Dessailly for their help extracting and using the PHYSAT outputs,
209 and Eric Pape for useful comments and text edits. The box plots in Fig. 3 were generated using
210 the IoSR Matlab toolbox (<https://github.com/IoSR-Surrey/MatlabToolbox>), and maps displayed
211 using m_map (<https://www.eoas.ubc.ca/~rich/map.html>).

212 **Author Contributions Statement**

213 M.M. conceived and designed the study, with input from A.P., A.D., and S.A. M.M. developed
214 the IME algorithm with input from A.P. and A.D., performed the data analyses, and led the
215 interpretations and writing. S.A. provided the PHYSAT outputs. A.P., A.D., E.M., and S.A.
216 provided significant input on the text, and contributed to discussions that shaped the study and
217 the manuscript.

218 **Competing Interests Statement**

219 The authors declare no competing interests.

220 **Tables**

	All IMEs	IMEs with Chl increase nearby islands $\geq 10\%$
IME prevalence		
Percentage of islands with IME detected at least one month a year	98.9%	90.1%
... at least 6 months a year	93.2%	55.1%
... year-long	44.3%	23.9%
Percentage of IME detections over all possible cases (664 islands, 12 months)	83.7%	54.2%
IME spatial impact		
Average IME area	8,001 km ²	13,558 km ²
Total IME area within the tropical Pacific (in percentage)	3,179,873 km ² (3.2%)	3,033,672 km ² (3.1%)
IME impact on surface chlorophyll concentration (Chl)		
Average nearby percentage Chl increase (pixels closest to island)	25.6%	40.8%
Average percentage Chl increase per IME	9.3%	13.1%
Average total Chl increase per IME (summed over the IME area)	0.21 tons/m	0.37 tons/m
Total IME-induced Chl increase in the tropical Pacific (in percentage)	83 tons/m (0.68%)	82 tons/m (0.67%)
IME impact on primary production (PP)		
Average percentage PP increase per IME	2.8%	4.2%
Average total PP increase per IME (summed over the IME area)	0.14 TgC/yr	0.23 TgC/yr
Total IME-induced PP increase in the tropical Pacific (in percentage)	50.4 TgC/yr (0.51%)	50.2 TgC/yr (0.51%)
IME impact on PHYSAT phenoclass diversity		
Average percentage richness increase per IME	12.1%	13.2%
Average percentage evenness increase per IME	-0.1%	0.0%
Average percentage Shannon index increase per IME	4.1%	4.5%

221 **Table 1: IME impacts in the tropical Pacific.** IME prevalence is defined based on islands
 222 belonging to an IME region (there can be several islands associated with one IME region).
 223 “Average” impact refers to impact for a single IME, averaged over all detected IMEs. They
 224 include both change in ambient conditions in IME vs REF regions, and total island-driven
 225 increase summed over the IME area. “Total” impact refers to impacts summed over the entire
 226 study region and averaged over a climatological year. Phenoclass diversity impacts were
 227 computed for IME/REF regions of at least 100 PHYSAT data points, and richness was

228 normalized to 100 data points to correct for the strong dependence of richness on area sampled
229 (see Methods). Statistics are given for all IMEs, and for a more conservative subset excluding
230 those where the island nearby Chl increase was below 10%. Additional metrics (median and
231 interquartile range) are provided in Extended Table 1.

232 **Figure legends**

233 **Figure 1: Map of IME detection in the tropical Pacific.** The main map represents the 2002-
234 2018 average satellite chlorophyll concentration (MODIS data) in the study region (30°S -
235 30°N). IME regions are contoured in different shades of red depending on Chl increase nearby
236 islands relative to a reference region (maximum value in mean conditions: 558% observed for the
237 Galapagos Islands). Inserts display the climatological month with the highest IME chlorophyll
238 enrichment in selected regions with a custom color bar: A- Kiribati in May, B- Hawaii in
239 September, C- Galapagos in January, D- Solomon in July, E- New Caledonia, Vanuatu, Fiji, and
240 Tonga in February, and F- Marquesas in May. Extended Fig. 2 provides full maps of
241 climatological months.

242 **Figure 2: Maps of island impacts on PHYSAT phenoclasses, indicative of impacts on**
243 **phytoplankton community composition and biodiversity.** For each island, the maximum value
244 observed over the seasonal cycle is displayed (only computed for IME regions containing at least
245 100 PHYSAT data points). a) Phenoclass Bray-Curtis dissimilarity between IME and REF
246 regions, indicative of differences in phenoclass composition. b) Phenoclass richness increases in
247 the IME region relative to REF (richness was normalized to 100 data points). c) Summary of
248 island impacts on phenoclasses, defined according to the median value for phenoclass Bray-
249 Curtis dissimilarity (composition, pink) and for richness increase (richness, blue), where
250 “impacts” are defined as above the median. Phenoclass richness increase is correlated with
251 absolute latitude ($r = 0.18$) while phenoclass Bray-Curtis dissimilarity is anticorrelated ($r = -$
252 0.24). Despite their opposite relation to latitude, phenoclass richness increase and Bray-Curtis
253 dissimilarity are actually weakly correlated ($r = 0.30$).

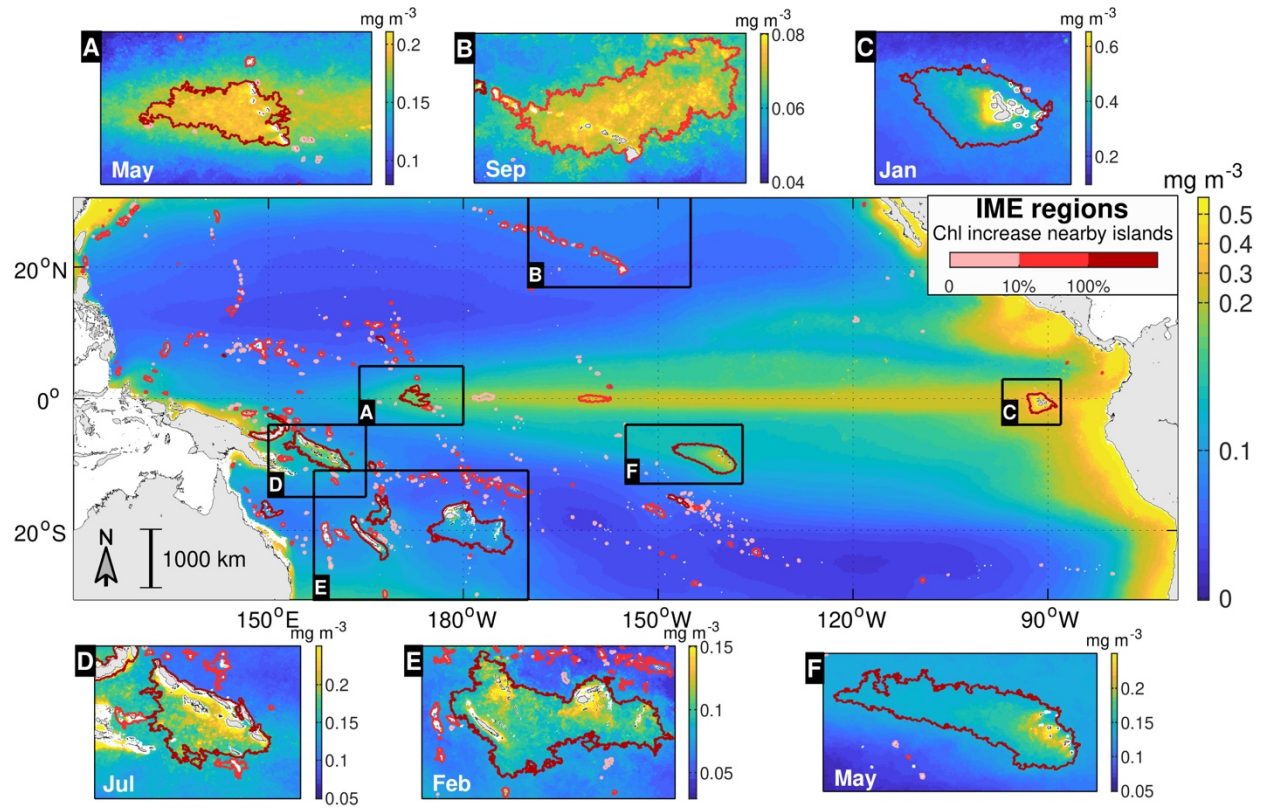
254 **Figure 3: Island impacts on phytoplankton community structure as depicted by PHYSAT.**

255 Statistics are based on paired climatological IME/REF regions with 100 PHYSAT data points
256 minimum. Box plots report the median (center line), 95% confidence interval around the median
257 (notches equal to ± 1.58 times interquartile range divided by square root of the sample size),
258 interquartile range (box), and 1.5 times the interquartile range (whiskers). Data points are
259 displayed as crosses (outliers beyond whiskers as dots). Symbols show whether distributions are
260 statistically different according to a Mann-Whitney U-test (= is non-significant, +/- indicate how
261 IME medians relate to REF).

262 **a)** Left: Phenoclass Bray-Curtis dissimilarity between IME and REF regions, compared to data
263 points randomly taken across IME/REF regions. Right: Occurrence frequency of dominant
264 phenoclasses (frequency >0.02) in the IME and REF regions, sorted by label: *Prochlorococcus*
265 (Pros), *Synechococcus* (Syn), and nanoplankton (Nano).

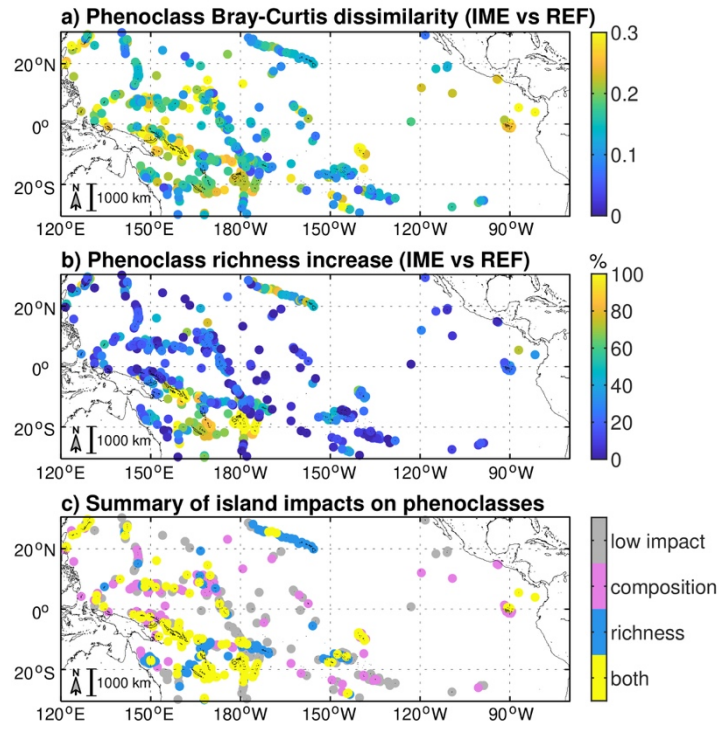
266 **b)** Left 2 panels: Phenoclass richness is significantly higher in IME than in REF regions (9.6%
267 difference in median) partly linked to higher Chl (12.4% difference in median). Right: summary
268 of Chl and phenoclass richness characteristics for 1000 random permutations independently
269 taken within IME and REF regions (N=712) such that their Chl distribution is equivalent
270 ($p>0.05$). Chl may be insignificantly higher within IME or REF subsets (as described by the
271 difference in median) because IME/REF pairs are decoupled (example in Extended Fig. 4).

272



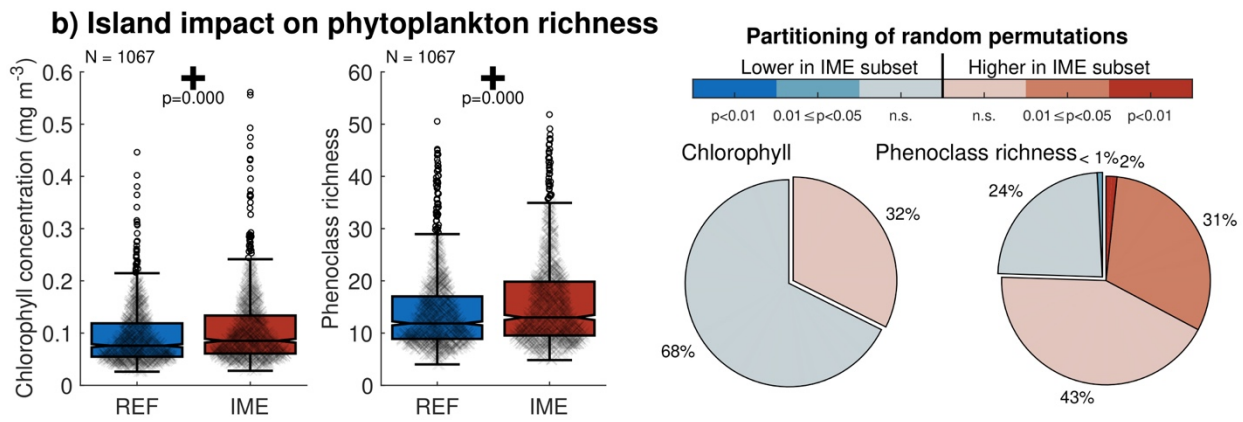
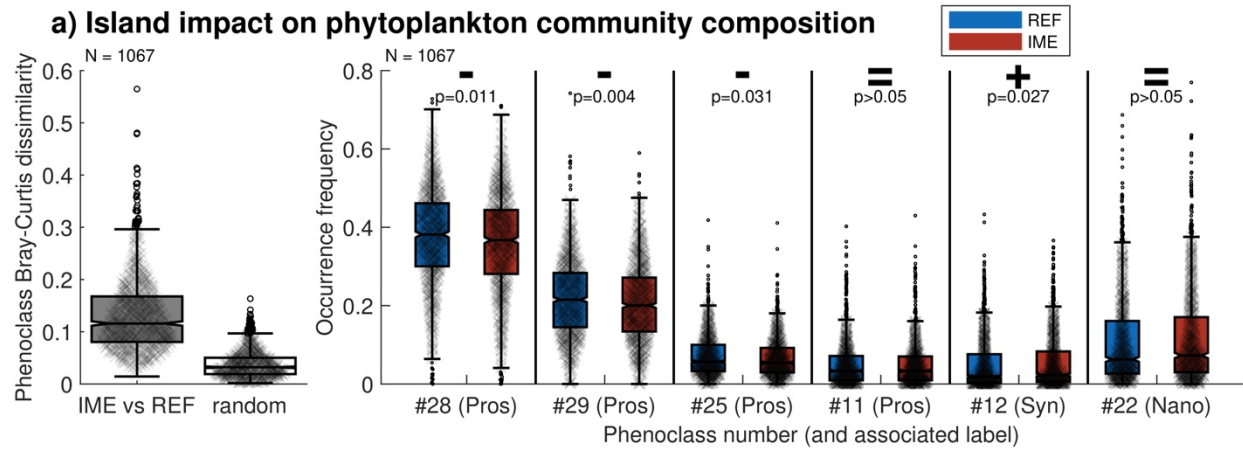
273
274
275

Figure 1.



276
 277
 278

Figure 2.



279

280

Figure 3.

281 **References**

- 282 1. Field, C. B., M. J. Behrenfeld, J. T. Randerson & P. Falkowski (1998), Primary production of
283 the biosphere: integrating terrestrial and oceanic components, *Science*, 281(5374), 237-240,
284 <https://doi.org/10.1126/science.281.5374.237>
- 285 2. Guidi, L., S. Chaffron, L., Bittner, D. Eveillard, A. Larhlimi, S. Roux et al. (2016), Plankton
286 networks driving carbon export in the oligotrophic ocean, *Nature*, 532(7600), 465-470,
287 <https://doi.org/10.1038/nature16942>
- 288 3. Ptacnik, R., A. G. Solimini, T. Andersen, T. Tamminen, P. Brettum, L. Lepistö, E. Willén &
289 S. Rekolainen (2008), Diversity predicts stability and resource use efficiency in natural
290 phytoplankton communities, *Proc. Natl. Acad. Sci.*, 105(13), 5134-5138,
291 <https://doi.org/10.1073/pnas.0708328105>
- 292 4. Corcoran, A. A. & W. J. Boeing (2012), Biodiversity increases the productivity and stability
293 of phytoplankton communities, *PLoS ONE*, 7(11), e49397,
294 <https://doi.org/10.1371/journal.pone.0049397>
- 295 5. Arteaga, L., M. Pahlow & A. Oschlies (2014), Global patterns of phytoplankton nutrient and
296 light colimitation inferred from an optimality-based model, *Global Biogeochem. Cycles*,
297 28(7), 648-661, <https://doi.org/10.1002/2013GB004668>
- 298 6. Lewis, M., D. Hebert, W. G. Harrison, T. Platt & N. S. Oakey (1986), Vertical nitrate fluxes in
299 the oligotrophic ocean, *Science*, 234(4778), 870-873,
300 <https://doi.org/10.1126/science.234.4778.870>

- 301 7. McGillicuddy, D. J. J., A. A. Laurence, N. R. Bates, T. Bibby, K. O. Buesseler, C. A. Carlson
302 et al. (2007), Eddy/wind interactions stimulate extraordinary mid-ocean plankton blooms,
303 Science, 316(5827), 1021-1026, <https://doi.org/10.1126/science.1136256>
- 304 8. Duce, R. A., J. LaRoche, K. Altieri, K. R. Arrigo, A. R. Baker, D. G. Capone et al. (2008),
305 Impacts of atmospheric anthropogenic nitrogen on the open ocean, Science, 320(5878), 893-
306 897, <https://doi.org/10.1126/science.1150369>
- 307 9. Tang, W., S. Wang, D. Fonseca-Batista, F. Dehairs, S. Gifford, A. G. Gonzalez et al. (2019),
308 Revisiting the distribution of oceanic N₂ fixation and estimating diazotrophic contribution to
309 marine production, Nat. Commun., 10(1), <https://doi.org/10.1038/s41467-019-08640-0>
- 310 10. Letscher, R. T., F. Primeau & J. K. Moore (2016), Nutrient budgets in the subtropical ocean
311 gyres dominated by lateral transport, Nat. Geosci., 9(11), 815-819,
312 <https://doi.org/10.1038/ngeo2812>
- 313 11. Righetti, D., M. Vogt, N. Gruber, A. Psomas & N. E. Zimmermann (2019), Global pattern of
314 phytoplankton diversity driven by temperature and environmental variability, Sci. Adv., 5(5),
315 eaau6253, <https://doi.org/10.1126/sciadv.aau6253>
- 316 12. Ibarbalz, F. M., Henry, N., Brandão, M. C., Martini, S., Busseni, G., Byrne, H. et al. (2019),
317 Global trends in marine plankton diversity across kingdoms of life, Cell, 179(5), 1084-
318 1097.e21, <https://doi.org/10.1016/j.cell.2019.10.008>
- 319 13. Lévy, M., P. J. S. Franks & K. S. Smith (2018), The role of submesoscale currents in
320 structuring marine ecosystems, Nat. Commun., 9(1), [https://doi.org/10.1038/s41467-018-](https://doi.org/10.1038/s41467-018-07059-3)
321 [07059-3](https://doi.org/10.1038/s41467-018-07059-3)

- 322 14. Dutkiewicz, S., P. Cermeno, O. Jahn, M. J. Follows, A. E. Hickman, D. A. A. Taniguchi &
323 B. A. Ward (2020), Dimensions of marine phytoplankton diversity, *Biogeosciences*, 17(3),
324 609-634, <https://doi.org/10.5194/bg-17-609-2020>
- 325 15. Gove, J. M., M. A. McManus, A. B. Neuheimer, J. J. Polovina, J. C. Drazen, C. R. Smith et
326 al. (2016), Near-island biological hotspots in barren ocean basins, *Nat. Commun.*, 7, 10581,
327 <https://doi.org/10.1038/ncomms10581>
- 328 16. Doty, M. S. & M. Oguri (1956), The island mass effect, *J. Cons. Int. Explor. Mer.*, 22(1), 33-
329 37, <https://doi.org/10.1093/icesjms/22.1.33>
- 330 17. Bell, J. D., M. Kronen, A. Vunisea, W. J. Nash, G. Keeble, A. Demmke, S. Pontifex & S.
331 Andréfouët (2009), Planning the use of fish for food security in the Pacific, *Marine Policy*,
332 33(1), 64-76, <https://doi.org/10.1016/j.marpol.2008.04.002>
- 333 18. Bakker, D. C., M. C. Nielsdóttir, P. J. Morris, H. J. Venables & A. J. Watson (2007), The
334 island mass effect and biological carbon uptake for the subantarctic Crozet Archipelago,
335 *Deep Sea Research Part II: Topical Studies in Oceanography*, 54(18-20), 2174-2190,
336 <https://doi.org/10.1016/j.dsr2.2007.06.009>
- 337 19. Heywood, K. J., D. P. Stevens & G. R. Bigg (1996), Eddy formation behind the tropical
338 island of Aldabra, *Deep Sea Res. Part I*, 43(4), 555-578, [https://doi.org/10.1016/0967-](https://doi.org/10.1016/0967-0637(96)00097-0)
339 [0637\(96\)00097-0](https://doi.org/10.1016/0967-0637(96)00097-0)
- 340 20. Palacios, D. M. (2002), Factors influencing the island-mass effect of the Galapagos
341 archipelago, *Geophys. Res. Lett.*, 29(23), 2134, <https://doi.org/10.1029/2002GL016232>

- 342 21. Gilmartin, M. & N. Revelante (1974), The 'island mass' effect on the phytoplankton and
343 primary production of the Hawaiian Islands, *J. Exp. Mar. Biol. Ecol.*, 16(2), 181-204,
344 [https://doi.org/10.1016/0022-0981\(74\)90019-7](https://doi.org/10.1016/0022-0981(74)90019-7)
- 345 22. Signorini, S. C., C. R. McClain & Y. Dandonneau (1999), Mixing and phytoplankton bloom
346 in the wake of the Marquesas Islands, *Geophys. Res. Lett.*, 26(20), 3121-3124,
347 <https://doi.org/10.1029/1999GL010470>
- 348 23. Messié, M., M.-H. Radenac, J. Lefèvre & P. Marchesiello (2006), Chlorophyll bloom in the
349 western Pacific at the end of the 1997-98 El Niño: the role of the Kiribati Islands, *Geophys.*
350 *Res. Lett.*, 33, L14601, <https://doi.org/10.1029/2006GL026033>
- 351 24. Messié, M. & M.-H. Radenac (2006), Seasonal variability of the surface chlorophyll in the
352 western tropical Pacific from SeaWiFS data, *Deep Sea Res. Part I*, 53(10), 1581-1600,
353 <https://doi.org/10.1016/j.dsr.2006.06.007>
- 354 25. Le Borgne, R., Y. Dandonneau & L. Lemasson (1985), The problem of the island mass effect
355 on chlorophyll and zooplankton standing crops around Mare (Loyalty Islands) and New
356 Caledonia, *Bull. Mar. Sci.*, 37(2), 450-459
- 357 26. Messié, M., A. Petrenko, A. M. Doglioli, C. Aldebert, E. Martinez, G. Koenig, S. Bonnet &
358 T. Moutin (2020), The delayed island mass effect: How islands can remotely trigger blooms
359 in the oligotrophic ocean, *Geophys. Res. Lett.*, 47(2), <https://doi.org/10.1029/2019gl085282>
- 360 27. Dandonneau, Y. & L. Charpy (1985), An empirical approach to the island mass effect in the
361 south tropical Pacific based on sea surface chlorophyll concentrations, *Deep Sea Research*
362 *Part A*, 32, 707-721, [https://doi.org/10.1016/0198-0149\(85\)90074-3](https://doi.org/10.1016/0198-0149(85)90074-3)

- 363 28. Shiozaki, T., T. Kodama & K. Furuya (2014), Large-scale impact of the island mass effect
364 through nitrogen fixation in the western South Pacific Ocean, *Geophys. Res. Lett.*, 41(8),
365 2907-2913, <https://doi.org/10.1002/2014GL059835>
- 366 29. Caputi, L., Q., Carradec, D., Eveillard, A., Kirilovsky, E., Pelletier, J. J. P. Karlusich et al.
367 (2019), Community-level responses to iron availability in open ocean plankton ecosystems,
368 *Global Biogeochem. Cycles*, 33(3), 391-419, <https://doi.org/10.1029/2018gb006022>
- 369 30. Martinez, E., M. Rodier, M. Pagano & R. Sauzède (2020), Plankton spatial variability within
370 the Marquesas archipelago, South Pacific, *J. Mar. Syst.*, 212, 103432,
371 <https://doi.org/10.1016/j.jmarsys.2020.103432>
- 372 31. Behrenfeld, M. J. & P. G. Falkowski (1997), Photosynthetic rates derived from satellite-
373 based chlorophyll concentration, *Limnol. Oceanogr.*, 42(1), 1-20,
374 <https://doi.org/10.4319/lo.1997.42.1.0001>
- 375 32. Laws, E. A., H. Ducklow & J. J. McCarthy (2000), Temperature effects on export production
376 in the open ocean, *Global Biogeochem. Cycles*, 14(4), 1231-1246,
377 <https://doi.org/10.1029/1999GB001229>
- 378 33. Messié, M. & F. P. Chavez (2012), A global analysis of ENSO synchrony: the oceans'
379 biological response to physical forcing, *J. Geophys. Res.*, 117, C09001,
380 <https://doi.org/10.1029/2012JC007938>
- 381 34. Luo, Y.-W., I. D. Lima, D. M. Karl, C. A. Deutsch & S. C. Doney (2014), Data-based
382 assessment of environmental controls on global marine nitrogen fixation, *Biogeosciences*,
383 11(3), 691-708, <https://doi.org/10.5194/bg-11-691-2014>

- 384 35. Messié, M. & F. P. Chavez (2015), Seasonal regulation of primary production in eastern
385 boundary upwelling systems, *Prog. Oceanogr.*, 134, 1-18,
386 <https://doi.org/10.1016/j.pocean.2014.10.011>
- 387 36. Mouw, C. B., N. J. Hardman-Mountford, S. Alvain, A. Bracher, R. J. W. Brewin, A. Bricaud
388 et al. (2017), A Consumer's guide to satellite remote sensing of multiple phytoplankton
389 groups in the global ocean, *Front. Mar. Sci.*, 4, 41, <https://doi.org/10.3389/fmars.2017.00041>
- 390 37. Alvain, S., C. Moulin, Y. Dandonneau & F. M. Bréon (2005), Remote sensing of
391 phytoplankton groups in case 1 waters from global SeaWiFS imagery, *Deep Sea Res. Part I*,
392 52(11), 1989-2004, <https://doi.org/10.1016/j.dsr.2005.06.015>
- 393 38. Rêve-Lamarche, A.-H., S. Alvain, M.-F. Racault, D. Dessailly, N. Guiselin, C. Jamet, V.
394 Vantrepotte & G. Beaugrand (2017), Ocean Color Radiance Anomalies in the North Sea,
395 *Front. Mar. Sci.*, <https://doi.org/10.3389/fmars.2017.00408>
- 396 39. Alvain, S., H. Loisel & D. Dessailly (2012), Theoretical analysis of ocean color radiances
397 anomalies and implications for phytoplankton groups detection in case 1 waters, *Opt.*
398 *Express*, 20(2), 1070, <https://doi.org/10.1364/oe.20.001070>
- 399 40. Mackey, D. J., J. Blanchot, H. W. Higgins & J. Neveux (2002), Phytoplankton abundances
400 and community structure in the equatorial Pacific, *Deep Sea Res. Part II*, 49(13-14), 2561-
401 2582, [https://doi.org/10.1016/S0967-0645\(02\)00048-6](https://doi.org/10.1016/S0967-0645(02)00048-6)
- 402 41. Johnson, Z. I. (2006), Niche partitioning among *Prochlorococcus* ecotypes along ocean-scale
403 environmental gradients, *Science*, 311(5768), 1737-1740,
404 <https://doi.org/10.1126/science.1118052>

- 405 42. Martiny, A. C., S. Kathuria & P. M. Berube (2009), Widespread metabolic potential for
406 nitrite and nitrate assimilation among *Prochlorococcus* ecotypes, *Proc. Natl. Acad. Sci.*,
407 106(26), 10787-10792, <https://doi.org/10.1073/pnas.0902532106>
- 408 43. Vallina, S. M., M. J. Follows, S. Dutkiewicz, J. M. Montoya, P. Cermeno & M. Loreau
409 (2014), Global relationship between phytoplankton diversity and productivity in the ocean,
410 *Nat. Commun.*, 5(1), <https://doi.org/10.1038/ncomms5299>
- 411 44. Dai, S., Y. Zhao, X. Li, Z. Wang, M. Zhu, J. Liang, et al. (2020), The seamount effect on
412 phytoplankton in the tropical western Pacific, *Mar. Environ. Res.*, 105094,
413 <https://doi.org/10.1016/j.marenvres.2020.105094>
- 414 45. Leitner, A. B., A. B. Neuheimer & J. C. Drazen (2020), Evidence for long-term seamount-
415 induced chlorophyll enhancements, *Sci. Rep.*, 10(1), [https://doi.org/10.1038/s41598-020-](https://doi.org/10.1038/s41598-020-69564-0)
416 [69564-0](https://doi.org/10.1038/s41598-020-69564-0)
- 417 46. Bowen, B. W., L. A. Rocha, R. J. Toonen & S. A. Karl (2013), The origins of tropical marine
418 biodiversity, *Trends in Ecology & Evolution*, 28(6), 359-366,
419 <https://doi.org/10.1016/j.tree.2013.01.018>
- 420 47. Worm, B., H. K. Lotze & R. A. Myers (2003), Predator diversity hotspots in the blue ocean,
421 *Proc. Natl. Acad. Sci.*, 100(17), 9884-9888, <https://doi.org/10.1073/pnas.1333941100>
- 422 48. Block, B. A., I. D., Jonsen, S. J., Jorgensen, S. A., Winship, S. A., Shaffer, S. J. Bograd et al.
423 (2011), Tracking apex marine predator movements in a dynamic ocean, *Nature*, 475, 86-90,
424 <https://doi.org/10.1038/nature10082>

- 425 49. Harrison, A.-L., D. P. Costa, A. J. Winship, S. R. Benson, S. J. Bograd, M. Antolos et al.
426 (2018), The political biogeography of migratory marine predators, *Nature Ecology &*
427 *Evolution*, 2(10), 1571-1578, <https://doi.org/10.1038/s41559-018-0646-8>
- 428 50. Pompa, S., P. R. Ehrlich & G. Ceballos (2011), Global distribution and conservation of
429 marine mammals, *Proc. Natl. Acad. Sci.*, 108(33), 13600-13605,
430 <https://doi.org/10.1073/pnas.1101525108>
431

432 **Methods**

433 **IME detection data sets.** The IME was detected from a climatology of MODIS satellite surface
434 chlorophyll-*a* concentrations (Chl, 4 km, monthly from July 2002 to December 2018,
435 erdMHIchlamday product downloaded from
436 <https://coastwatch.pfeg.noaa.gov/erddap/info/index.html>). The study was based on the 4 km
437 MODIS Chl grid in the tropical Pacific (30°N/30°S; east/west borders are roughly delimited by
438 the Americas, Australia, Indonesia, Philippines, and Taiwan, see Fig. 1). Islands were detected
439 from the Global Self-consistent, Hierarchical, High-resolution Geography Database (GSHHG)
440 version 2.3.7 full resolution coastline (<https://www.ngdc.noaa.gov/mgg/shorelines/gshhs.html>)
441 loaded using functions from the m_map toolbox (<https://www.eoas.ubc.ca/~rich/map.html>).
442 Bathymetry was obtained from the GEBCO global bathymetry
443 (https://www.gebco.net/data_and_products/gridded_bathymetry_data/) at 1/15' resolution (< 500
444 m). A 4 km resolution “shallow mask” was generated for the MODIS grid, including all pixels
445 containing land shallower than 30 m according to GEBCO or where an island was detected. The
446 shallow mask was extended by one additional pixel in all directions to ensure that all pixels
447 containing shallow waters were flagged¹⁵. All ocean color data (Chl, primary production, and
448 PHYSAT, see below) were removed within the shallow mask as they were potentially
449 contaminated by bottom reflectance¹⁵. In practice, pixels within the shallow mask (containing
450 land, waters shallower than 30 m, and adjacent pixels) were treated as land.

451 **Island database.** The island database includes both emerged islands and reefs shallower than 30
452 m according to the GEBCO bathymetry. The reason is that some atolls can have no consistent
453 (e.g., tide-dependent) or very little emerged land, and can potentially be missed both by GSHHG
454 and by the GEBCO bathymetry. Islands and reefs were identified as follows. Islands were

455 detected from the GSHHS coastline as closed contours in the 120°E-70°W, 30°S-30°N region.
456 Because GSHHG was constructed from databases that were built in the 70s and 80s, errors
457 remained in the location of some islands. Islands being too numerous to all be validated, only
458 islands from the final database (see below) were checked against GEBCO bathymetry, and where
459 obvious discrepancies existed, their position was shifted accordingly. The island database was
460 then reprocessed until no more discrepancy was found (total corrected islands: n=32). The island
461 database was merged with a published database of 1,779 islands⁵¹ by finding, for each island
462 from the Nunn et al. database⁵¹, the closest GSHHS contour. The Nunn et al. database⁵¹ provides
463 more precise information regarding position, elevation, island type, and area. Last, reefs were
464 detected from GEBCO (at < 500 m resolution) as groups of pixels shallower than 30 m (“shallow
465 zones”, n=5,972), that include both submerged reefs and emerged islands. Island and reef
466 databases were merged by finding islands within shallow zones, when they existed. The
467 combined dataset after removing contours within the east/west mask (e.g., Atlantic, Indonesia)
468 includes 16,051 islands and reefs (hereafter “islands”). Islands within 100 km of the tropical
469 Pacific east/west borders were removed to avoid continental influences (n=5,062). The remaining
470 islands were then combined within the MODIS shallow mask (see section above and Fig. S1).
471 The term “island” in the paper thus refers to a group of islands/reefs belonging to a set of
472 connected shallow pixels. The final database includes 664 islands (437 with emerged lands,
473 including 363 from the Nunn et al. island database⁵¹, and 227 shallow reefs).

474 **IME detection.** The IME was defined for each island as the smallest possible Chl contour
475 enclosing the island that fulfills a list of criteria detailed below (see Fig. S2 for a representation
476 of the algorithm). Beforehand, the maximum (Chl_max) and minimum (Chl_min) nearby Chl
477 were obtained for each island within a 1-pixel band around the island mask. Islands were ranked

478 by Chl_min, and processed from lowest to highest Chl_min. For a given island, the IME Chl
479 contour (termed cChl) was iteratively lowered by 0.01 mg m⁻³ starting at Chl_max and the
480 corresponding IME mask computed. The IME mask includes both pixels above cChl and
481 adjacent missing data, such that other islands can become part of the same IME, then termed
482 “shared IME”. When this happened, Chl_max was adjusted to the highest value; Chl_min does
483 not need adjustment since islands are processed in Chl_min order. The iteration was stopped
484 when one of the following conditions was met: (1) cChl < Chl_min (the rationale being that
485 currents displace the nutrient enrichment downstream of the island, so that at least one pixel
486 surrounding the island should not belong to the IME); (2) the IME mask was too large, either
487 touching the domain borders, or touching the continent masks or adjacent NaN pixels (this
488 happens when contours enclose the full oligotrophic gyre); (3) regions of high Chl (>
489 0.8*Chl_max) were found within the IME mask, further than 32 pixels away from any island
490 (~ 150 km). In this last case, the goal was to avoid non-island sources of nutrients within the IME
491 region such as open-ocean eddies or upwelling; the 32-pixel tolerance deals with cases where the
492 Chl maximum is displaced downstream of the islands⁵². The IME peak can occur even further
493 downstream, notably in cases of delayed IME²⁶; 32 pixels thus represents a compromise between
494 capturing most IMEs and avoiding non-IME local Chl enrichments. While sensitive to the
495 parameters used, this criterium only concerned 1.3% of cases (for the monthly climatology); in
496 95% of cases, the algorithm stops due to criterion #2. When one of the 3 criteria was met, a
497 second iteration was performed at higher resolution (0.001 mg m⁻³) starting with the last cChl
498 until meeting the criteria again, such that cChl was determined with a 0.001 mg m⁻³ accuracy.
499 This is well beyond measured Chl accuracy, but small changes in cChl can result in large
500 changes in IME areas on climatological averages, hence the need for high sensitivity. The IME

501 was only kept if the IME mask contained at least 2 Chl pixels. The IME detection algorithm is
502 available at https://bitbucket.org/messiem/toolbox_IME_detection.

503 **Satellite-derived information on phytoplankton biomass and primary production.** Island
504 impacts were assessed using satellite chlorophyll-*a* (Chl), a common proxy for phytoplankton
505 biomass⁵³ representative of the top ~ 10-30 m in our region (first optical depth). Subsurface
506 impacts remain unknown; in some cases, apparent surface enrichments can result from the
507 passive uplift of the deep chlorophyll maximum without any net biomass increase⁵⁴. However, in
508 situ profiles available near islands suggest this is the exception rather than the rule¹⁵ (see also
509 Table S3). Island impacts on primary production were estimated using the MODIS-based
510 standard Vertically Generalized Production Model³¹ (VGPM). The VGPM estimates primary
511 production integrated over the euphotic depth range based on satellite chlorophyll, light
512 availability, and temperature (a proxy for nutrient availability), and has been widely used for
513 large-scale studies for which the spatiotemporal coverage of in situ data remains insufficient.
514 Results are similar when using a more recent primary production algorithm (CAFE model⁵⁵):
515 total IME-induced PP increase = 44.9 TgC/yr vs 50.4 TgC/yr for the VGPM (Table 1). Primary
516 production was downloaded from the Ocean Productivity website
517 (<http://science.oregonstate.edu/ocean.productivity/index.php>) at 9 km resolution for the period
518 July 2002 - December 2018 (see above for Chl data information). Primary production maps were
519 averaged into a monthly climatology, pixels shallower than 30 m removed, and data interpolated
520 on the Chl grid (4 km resolution). The lower resolution of the primary production product means
521 that areas larger than for Chl were impacted by the shallow pixel removal, effectively removing
522 high values near islands more than for Chl; the corresponding pixels on the Chl grid (i.e. outside
523 of the Chl shallow mask) were interpolated using a median filter.

524 **Island-driven impacts on chlorophyll and primary production.** Island impacts were assessed
525 by contrasting data in the IME region to data in a reference region (REF), defined as the closest
526 N pixels from the island mask that do not belong to any IME region, where N is the number of
527 pixels within the IME region excluding the shallow mask (Extended Fig. 1). When assessing the
528 island impact on variables other than chlorophyll (i.e. primary production or PHYSAT), the
529 region with the largest number of data pixels was adapted. Indeed, different datasets may have
530 different data gaps, thus changing the number of data points in each region. To ensure that the
531 number of data points remained identical in both regions, the region with most pixels was
532 randomly subsampled to match the region with fewer pixels. The REF region was used to define
533 the nearby Chl increase for each island (Chl_max relative to average Chl within REF). Detecting
534 IMEs using a high sensitivity is justified on a climatological basis where spatial variability is
535 heavily smoothed by a 17-year average; however, weak increases could result from noise.
536 Statistics in Table 1 are thus presented both for all IMEs (more exhaustive) and after excluding
537 IMEs with Chl increases near islands below 10% (more conservative).

538 **PHYSAT.** The PHYSAT method³⁷ is based on daily, 4-km resolution normalized water-leaving
539 radiance (primary variable measured by a satellite ocean color radiometer after atmospheric
540 correction, for several wavelengths). First, spectral radiance anomalies (Ra) are computed by
541 removing a reference spectrum function of Chl for the same pixel, ensuring that the first order
542 chlorophyll signal is removed. Then, these anomalies are clustered using an automatic
543 unsupervised classification approach (self-organizing maps), classifying daily Ra into 100
544 “neuron groups” corresponding to a specific Ra spectral frequency shape and amplitude⁵⁶. The
545 number of neuron groups is reduced using phenological metrics to identify signals linked to
546 specific phytoplankton assemblages³⁸, termed “phenoclasses” (61 for PHYSAT applied to

547 MODIS-Aqua). A previous version of PHYSAT was applied to the SeaWiFS satellite and
548 matched with coincident *in situ* phytoplankton data, which enabled SeaWiFS phenoclasses to be
549 labeled with six broad phytoplankton groups⁵⁷. Phytoplankton labels are also available for
550 MODIS phenoclasses, through SeaWiFS/MODIS matchups during their overlapping period.
551 Around half of MODIS phenoclasses remain unlabeled, but could be matched to phytoplankton
552 groups as more samples become available. The most common phenoclasses present in the
553 tropical Pacific were labeled and found to be dominated by *Prochlorococcus*, *Synechococcus*,
554 and nanoplankton. Daily MODIS phenoclasses (4 km resolution, July 2002 - April 2018) were
555 averaged as a monthly climatology of phenoclass occurrence frequency at each pixel; pixels
556 shallower than 30 m were removed. The corresponding product was used to calculate the
557 phenoclass composition (percentage of occurrence for each phenoclass) within each IME and
558 REF region detected previously. Ecological metrics were only computed in IME and REF
559 regions including at least 100 PHYSAT data pixels, to ensure adequate PHYSAT coverage. This
560 represents around half of the detected IMEs.

561 **PHYSAT ecological metrics.** Classical ecological metrics were computed from phenoclass
562 proportions averaged in each IME and REF region, by regarding each phenoclass as a “species”
563 in mathematical equations for each index. In practice, each phenoclass can contain varying
564 numbers of species. However, phytoplankton richness is relatively stable in the tropics¹¹, so that
565 the number of phytoplankton species belonging to each phenoclass should be relatively constant.
566 Island impacts on phenoclass composition were assessed using the Bray-Curtis dissimilarity
567 index⁵⁸ between each pair of IME and REF regions. The Bray-Curtis index can vary between 0
568 and 1, where 0 would indicate that IME and REF have the same phenoclass composition, and 1
569 that they do not share any phenoclasses. Island impacts on phenoclass diversity were assessed

570 using various biodiversity metrics: richness, Pielou's evenness⁵⁹, and the Shannon index⁶⁰. These
571 metrics were computed in each IME and REF regions separately, and contrasted (similar to
572 chlorophyll and primary production). Just like true species richness strongly depends on
573 sampling effort, phenoclass richness increases with the number of pixels over which it is
574 computed (see Fig. S3). Phenoclass richness was corrected by rarefaction to 100 pixels to enable
575 direct statistical comparisons of richness across regions⁶¹. Computing biodiversity indices from
576 satellite products of phytoplankton taxonomy is not new. A previous study computed global
577 Shannon diversity metrics from PHYSAT six broad phytoplankton groups, identifying regional
578 hotspots matching known biodiversity hotspots⁶². While precise biodiversity estimates require an
579 extensive knowledge of the community, the De Monte index worked by capturing spatial
580 heterogeneity in dominant phytoplankton groups, which was shown to be highly correlated to
581 phytoplankton biodiversity in a model⁶³. Here, by applying a similar method but using all 61
582 phenoclasses, we are exploiting the full power of the PHYSAT algorithm and capturing a more
583 precise picture of changes in phytoplankton taxonomy and biodiversity. This is a very powerful
584 approach because it bypasses the need to identify phytoplankton taxonomy from space. While
585 PHYSAT is only a proxy for phytoplankton taxonomy, broad phenoclass diversity patterns match
586 published phytoplankton biodiversity patterns such as increasing richness with phytoplankton
587 biomass in unproductive waters⁴³ (Extended Fig. 3).

588 **Data availability statement**

589 The main outputs of this study, including the island database, IME and REF masks, and IME
590 impacts on chlorophyll, primary production, and PHYSAT, are available as a dataset hosted on
591 Zenodo⁶⁴. The PHYSAT climatology calculated for this paper is available there as well;
592 PHYSAT is now being processed by ACRI (<https://www.acri-st.fr/>) and PHYSAT data will soon
593 be publicly available from their website. Other data that support the findings of this study are
594 available in various public repositories: <https://coastwatch.pfeg.noaa.gov/erddap/info/index.html>
595 (MODIS chlorophyll concentration), <http://science.oregonstate.edu/ocean.productivity/index.php>
596 (MODIS primary production), <https://www.ngdc.noaa.gov/mgg/shorelines/gshhs.html> (GSHHG
597 coastline), https://www.gebco.net/data_and_products/gridded_bathymetry_data/ (GEBCO
598 bathymetry). The Nunn et al. (2016) island database is available as an additional file
599 accompanying their paper (<https://doi.org/10.1186/s40562-016-0041-8>).

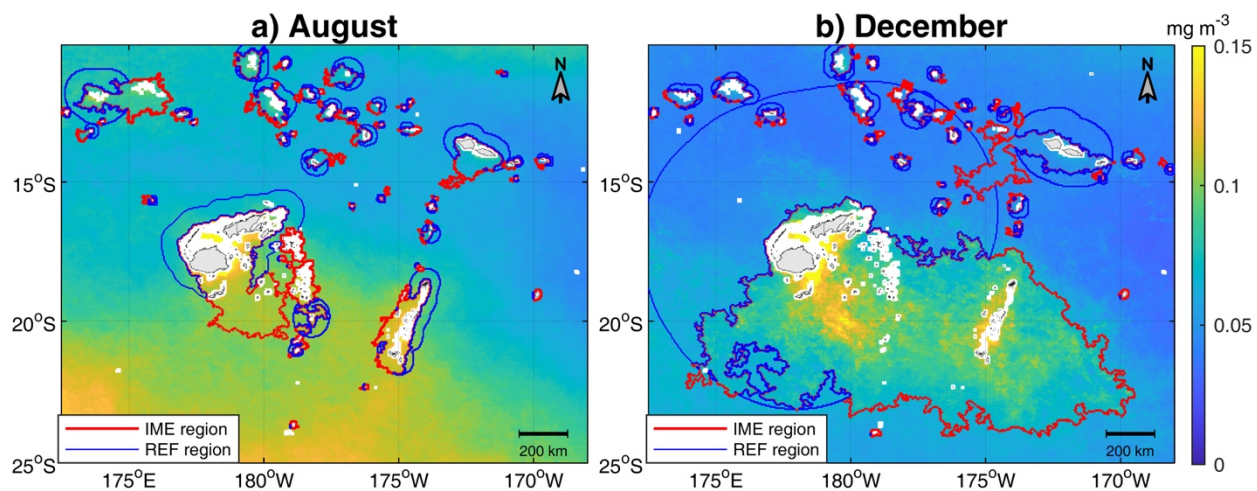
600 **Code availability statement**

601 The IME detection algorithm, along with datasets and example code to reproduce Fig. 1,
602 Extended Fig. 1, and parts of Table 1, is available at
603 https://github.com/messiem/toolbox_IME_detection and the corresponding release published on
604 Zenodo⁶⁵.

605 **Additional references for the Methods section**

- 606 51. Nunn, P. D., L. Kumar, I. Eliot & R. F. McLean (2016), Classifying Pacific islands,
607 Geoscience Letters, 3(1), <https://doi.org/10.1186/s40562-016-0041-8>
- 608 52. Hasegawa, D., M. R. Lewis & A. Gangopadhyay (2009), How islands cause phytoplankton
609 to bloom in their wakes, Geophys. Res. Lett., 36, L20605,
610 <https://doi.org/10.1029/2009GL039743>
- 611 53. Platt, T. & S. Sathyendranath (1988), Oceanic Primary Production: Estimation by Remote
612 Sensing at Local and Regional Scales, Science, 241(4873), 1613-1620,
613 <https://doi.org/10.1126/science.241.4873.1613>
- 614 54. Hasegawa, D., H. Yamazaki, T. Ishimaru, H. Nagashima & Y. Koike (2008), Apparent
615 phytoplankton bloom due to island mass effect, J. Mar. Sys., 69(3-4), 238-246,
616 <https://doi.org/10.1016/j.jmarsys.2006.04.019>
- 617 55. Silsbe, G. M., M. J. Behrenfeld, K. H. Halsey, A. J. Milligan & T. K. Westberry (2016), The
618 CAFE model: A net production model for global ocean phytoplankton, Glob. Biogeochem.
619 Cycles, 30(12), 1756-1777, <https://doi.org/10.1002/2016GB005521>
- 620 56. Ben Mustapha, Z., S. Alvain, C. Jamet, H. Loisel & D. Dessailly (2014), Automatic
621 classification of water-leaving radiance anomalies from global SeaWiFS imagery:
622 Application to the detection of phytoplankton groups in open ocean waters, Remote Sens.
623 Environ., 146, 97-112, <https://doi.org/10.1016/j.rse.2013.08.046>
- 624 57. Alvain, S., C. Moulin, Y. Dandonneau & H. Loisel (2008), Seasonal distribution and
625 succession of dominant phytoplankton groups in the global ocean: A satellite view, Glob.
626 Biogeochem. Cycles, 22(3), <https://doi.org/10.1029/2007GB003154>

- 627 58. Bray, J. R. & J. T. Curtis (1957), An Ordination of the Upland Forest Communities of
628 Southern Wisconsin, *Ecological Monographs*, 27(4), 325-349,
629 <https://doi.org/10.2307/1942268>
- 630 59. Pielou, E. (1966), The measurement of diversity in different types of biological collections, *J.*
631 *Theor. Biol.*, 13, 131-144, [https://doi.org/10.1016/0022-5193\(66\)90013-0](https://doi.org/10.1016/0022-5193(66)90013-0)
- 632 60. Shannon, C. & W. Weaver (1948), Biodiversity measurements, *The Mathematical Theory of*
633 *Communication*. Urbana University Press, Illinois, 117-27
- 634 61. Colwell, R. K., C. X. Mao & J. Chang (2004), Interpolating, extrapolating, and comparing
635 incidence-based species accumulation curves, *Ecology*, 85(10), 2717-2727,
636 <https://doi.org/10.1890/03-0557>
- 637 62. De Monte, S., A. Soccodato, S. Alvain & F. d'Ovidio (2013), Can we detect oceanic
638 biodiversity hotspots from space?, *The ISME Journal*, 7(10), 2054-2056,
639 <https://doi.org/10.1038/ismej.2013.72>
- 640 63. Soccodato, A., F. d'Ovidio, M. Lévy, O. Jahn, M. J. Follows & S. D. Monte (2016),
641 Estimating planktonic diversity through spatial dominance patterns in a model ocean, *Mar.*
642 *Geonomics*, 29, 9-17, <https://doi.org/10.1016/j.margen.2016.04.015>
- 643 64. Messié, M., A. Petrenko, A. Doglioli, E. Martinez & S. Alvain (2022), Data from: Basin-
644 scale biogeochemical and ecological impacts of islands in the tropical Pacific Ocean (v1.0.0),
645 Zenodo, <https://doi.org/10.5281/zenodo.6416130>
- 646 65. Messié, M. (2022), Code for: Basin-scale biogeochemical and ecological impacts of islands
647 in the tropical Pacific Ocean (v1.0.0), Zenodo, <https://doi.org/10.5281/zenodo.6494328>
- 648



649

650 **Extended Data Fig. 1: Example maps of IME and reference (REF) region detection. Two**

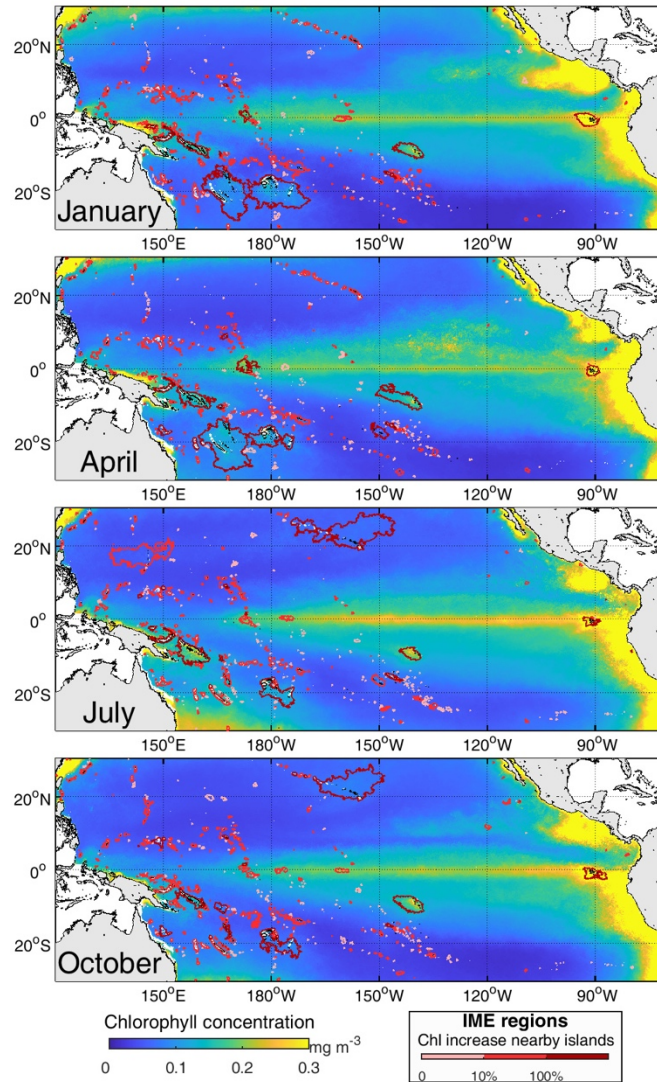
651 contrasting months are shown for the Fiji/Tonga region: a) August (small IMEs but higher

652 climatological enrichment across the region), and b) December (strong IMEs, with IMEs from

653 the Fiji and Tonga island groups merging). Reference regions (blue) exclude IME regions from

654 any island.

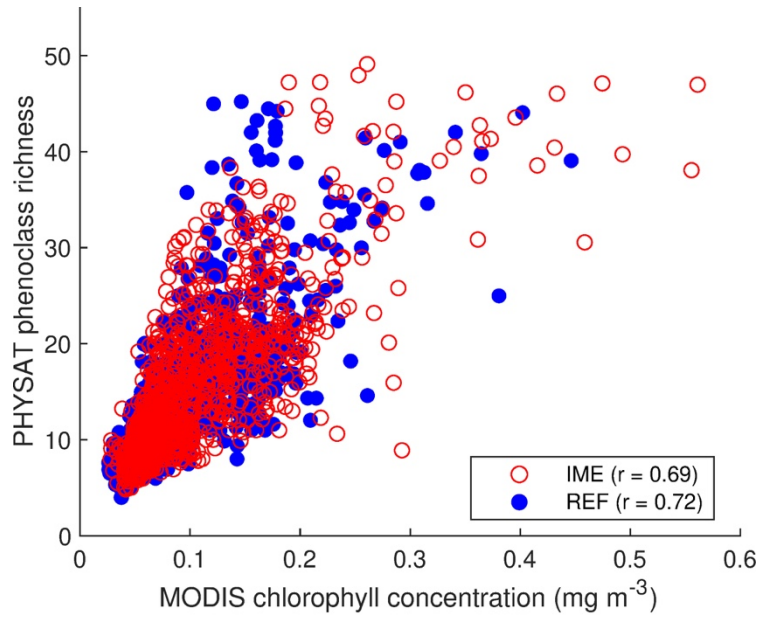
655



656

657 **Extended Data Fig. 2: IME maps for different climatological months.** For each month, IME
 658 regions are contoured in different shades of red depending on Chl increase near islands relative
 659 to a reference region (similar to Fig. 1).

660



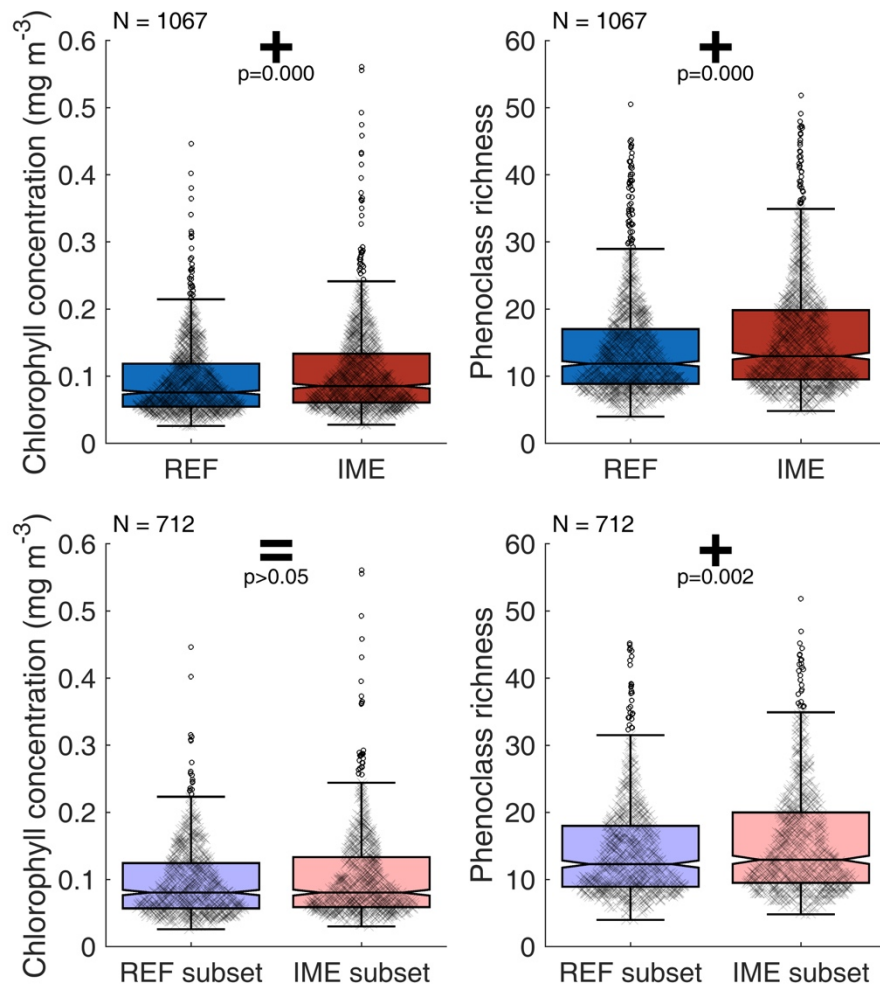
661

662 **Extended Data Fig. 3: PHYSAT phenoclass richness vs Chl across IME and REF regions.**

663 Phenoclass richness was normalized to 100 data points, and only regions with at least 100

664 PHYSAT data points were included.

665



666

667 **Extended Data Fig. 4: Example of random permutation used to remove the Chl signal on**
 668 **the phenoclass richness increase observed in IME regions.** Top panel: identical to Fig. 3b left
 669 panels (that is, including all IME and REF regions); both Chl (left) and phenoclass richness
 670 (right) are significantly higher in IME than in REF regions (Mann-Whitney U-test). Bottom
 671 panel: example of a random permutation where 2/3 of the IME and REF regions were retained
 672 such that the Chl distributions do not significantly differ anymore. In this permutation,
 673 phenoclass richness remains significantly higher within the IME subset (right) even though Chl
 674 is (non-significantly) lower (left).

675

	All IMEs	IMEs with Chl increase nearby islands $\geq 10\%$
IME spatial impact		
IME area (in km ²)	559 [172 – 2,051]	1,333 [430 – 3,965]
IME impact on Chl		
Nearby percentage Chl increase (in %)	11.4 [6.5 – 22.3]	19.9 [13.8 – 36.4]
Percentage Chl increase per IME (in %)	6.8 [4.4 – 10.8]	10.0 [7.3 – 14.2]
Total Chl increase per IME (in tons/m)	0.00 [0.00 – 0.01]	0.01 [0.00 – 0.04]
IME impact on primary production (PP)		
Percentage PP increase per IME (in %)	1.5 [0.3 – 3.5]	2.6 [0.9 – 5.3]
Total PP increase per IME (in TgC /yr)	0.00 [0.00 – 0.00]	0.00 [0.00 – 0.01]
IME impact on PHYSAT phenoclass diversity		
Percentage richness increase per IME (in %)	7.7 [-0.1 – 18.9]	8.9 [0.0 – 20.8]
Percentage evenness increase per IME (in %)	-0.3 [-6.4 – 6.0]	-0.3 [-6.6 – 6.2]
Percentage Shannon index increase per IME (in %)	2.9 [-1.7 – 8.7]	3.3 [-1.5 – 9.4]

676 **Extended Data Table 1: Additional metrics for IME impacts in the tropical Pacific (see**
677 **Table 1).** Values are given as median [25th percentile – 75th percentile]. The extremely low
678 values for total Chl and total primary production (intentionally kept in the same unit as in Table
679 1) highlight how a few major IMEs (visible in Fig. 1) are responsible for most of the large-scale
680 impact on Chl and primary production.